Characterizing close-focus lenses for microendoscopy

Dominique Galvez[a], **Zhihan Hong**[a], **Andrew D. Rocha**[a], **John M. Heusinkveld**[b], **Piaoran Ye**[c], **Rongguang Liang**[a], **and Jennifer K. Barton**[a,d,*]

[a]University of Arizona, Wyant College of Optical Sciences, Tucson, Arizona, United States
[b]University of Arizona, Department of Obstetrics and Gynecology, Tucson, Arizona, United States
[c]University of Arizona, Department of Chemistry and Biochemistry, Tucson, Arizona, United States
[d]University of Arizona, Department of Biomedical Engineering, Tucson, Arizona, United States

Abstract. Microendoscopes are commonly used in small lumens in the body for which a focus near to the distal tip and ability to operate in an aqueous environment are paramount for navigation and disease detection. Commercially available distal optic systems below 1 mm in diameter are severely limited, and custom micro lenses are generally very expensive. Gradient index of refraction (GRIN) singlets are available in small diameters but have limited optical performance adjustability. Three-dimensional (3D)-printed monolithic optical systems are an emerging option that may be suitable for enabling high performance, close-focus imaging. In this manuscript, we compared the optical performance of three custom distal optic systems; a custom-pitch GRIN singlet, 3D-printed monolithic doublet, and 3D-printed monolithic triplet, with a nominal working distance (WD) of 1.5, 0.5, and 0.4 mm in 0.9% saline. These short WDs are ideal for microendoscopy in collapsed or flushed lumens such as pancreatic duct or fallopian tube. The GRIN singlet had performance limited only by the fiber bundle relay over 0.9- to 1.6-mm depth of field (DOF). The 3D-printed doublet was able to achieve a comparable DOF of 0.71 mm, whereas the 3D-printed triplet suffered the most limited DOF of 0.55 mm. 3D printing enables flexible design of monolithic multielement systems with aspheric surfaces of very short WDs and relative ease of integration. © *The Authors. Published by SPIE under a Creative Commons Attribution 4.0 International License. Distribution or reproduction of this work in whole or in part requires full attribution of the original publication, including its DOI.* [DOI: 10.1117/1.JOM.3.1.011003]

Keywords: endoscopy; lens design; three-dimensional printing; microendoscope; multimodal imaging.

Paper 22020SS received Aug. 8, 2022; accepted for publication Dec. 19, 2022; published online Jan. 4, 2023.

1 Introduction

Minimally invasive endoscopic imaging offers the opportunity for early detection of cancer and other disease states by bringing powerful optical techniques to the interior of the body. For example, in one study colonoscopy was associated with a 61% reduction in colon cancer mortality among veterans.[1] However, the colon has a large lumen, accommodating endoscopes of around 12 mm in diameter, which typically includes imaging lenses in the 2- to 3-mm-diameter range. The desire to extend minimally invasive clinical imaging to organs with smaller lumens, such as the pancreas,[2] fallopian tube,[3] bronchioles,[4] or guiding needle biopsies of the lungs[5] or during neurosurgery,[6] has necessitated the development of microendoscopes that are submillimeter in diameter. These endoscopes may contain one or more imaging modalities and possibly other functionalities, such as cell/tissue collection, laser therapy, or drug delivery. In these microendoscopes, optical channel diameters are limited to the 100- to 500-μm-diameter range. The small

*Address all correspondence to Jennifer K. Barton, barton@arizona.edu

lumens themselves define a new set of challenges that drive specialized lens requirements. Typical endoscope optics for large cavities or lumens have moderate to large angular fields of view (AFOV) and are designed for operation in an air or insufflation gas environment and focused at the hyperfocal distance, from a few millimeters to infinity. However, small lumens may be collapsed and filled with mucus, cilia, or plicae. Therefore, it is more likely that microendoscopes will need moderate AFOV, depth of field (DOF) from less than a millimeter to a few millimeters, and ability to operate in an environment where 0.9% saline is used for flushing and irrigation as an immersion objective. We are particularly interested in distal optic systems of 0.5 mm or less in diameter that can operate in these cramped aqueous environments.

There are two main detection options for microendoscopic imaging, a distal miniature sensor (recently dubbed the "chip-on-tip") or a fiber image guide, which directs light to a remote possibly high-sensitivity and relatively large complementary metal oxide semiconductor (CMOS) or charge-coupled device (CCD) camera. The chip-on-tip technology powered by a new generation of micro-CMOS detectors is applicable to submillimeter diameter endoscopes, but these sensors are still too large for multimodality or multifunctional microendoscopes. Fiber image guides with 1000 to 10,000 cores are appropriate for situations where the imaging channel should be 500 μm or less in diameter and/or where a highly sensitive camera is required.

With either of these options, corresponding 100- to 500-μm-diameter optical elements must be used to focus the image onto the fiber guide or miniature detector. Optical elements manufactured in a variety of ways can be used. Glass catalog optics with diameters smaller than 1 mm are rare, but specialty optics companies can use conventional lens grinding procedures to create custom miniature optics. The advantage of this approach is that a large variety of materials can be used together with well-established optical design methods. For example, we previously demonstrated a custom 300-μm-diameter triplet distal optic system consisting of two plano-convex and a meniscus lens made from glasses and sapphire, with excellent optical performance.[7] The disadvantages of this method are the high cost and challenging assembly of multielement systems.

Gradient index of refraction (GRIN) rod lenses are readily available in 0.5 mm or smaller diameters to be used as a singlet. Their ease of assembly, a cylindrical rod shape abutting the end of a fiber bundle or miniature sensor, makes them an attractive choice for miniature endoscopes. Commercial off-the-shelf GRIN lenses used as a singlet objective generally have too long of a working distance (WD) for a microendoscope, but custom pitch (length) GRIN singlets can be obtained at a relatively low cost, or a GRIN microendoscope system for a higher cost. However, GRIN singlet systems have limited optical parameters that can be varied (gradient parameter and pitch) and typically suffer from strong chromatic aberration as a lone element. In regards to microendoscope biocompatibility, care must be taken that the GRIN material and dopants are either nontoxic or the GRIN lens is coated/covered with a biocompatible material.[8] Use of a GRIN singlet system with fiber bundles is common and our group has previously demonstrated the use of a 0.25-mm-diameter GRIN singlet with 3000 element fiber bundles for imaging of the fallopian tubes.[9,10] Optical performance limitations of a GRIN singlet has been mitigated through additional optical elements placed in proximity to, or manufactured directly on, the GRIN element. For example, an epoxy window was created with soft lithography[11] to correct a GRIN-fiber-based optical coherence tomography (OCT) probe, and a three dimensional (3D) printed correction surface for the proximal end of a GRIN-rod-based two-photon microscopy system[12] has been demonstrated. Nanopatterned metasurfaces[13] and 3D-printed off-axis freeform total internal reflection mirrors[14] are further methods for creating miniature optical systems and have been combined with fiber optics to create OCT fiber probes with high resolution over extended DOF. The flexibility afforded by 3D-printing is beginning to be more widely utilized in endoscope optics. For example, a monolithic optical design for OCT and fluorescence microendoscopy has been demonstrated.[15] Relevant to *en face* imaging with fiber bundles or miniature sensors, we previously demonstrated a 0.5-mm-diameter 3D-printed singlet lens that showed large DOF and excellent surface quality,[16] however bulk scattering of the resin material degraded optical performance.

Recent activity has focused on expanding 3D-printed lens material beyond the resins typically used. Liquid silica resin (LSR) has recently been introduced and is an exciting option due to the potential for biocompatibility and higher ultraviolet (UV)/blue transmission where other

typically used resins may absorb.[17,18] However, it is important to note that the 3D printing fidelity of precision glass optics for imaging applications is still limited by its shrinkage and highly controlled surface accuracy during manufacturing. 3D printing allows for the design of monolithic optical systems, simplifying the alignment process of coupling to a fiber bundle or sensor, and an optical stop can be incorporated directly into the lens system. Most importantly, the proposed printing strategy significantly increases the flexibility of the design and fabrication of miniature aspheric optics, which are currently unachievable with conventional grinding and polishing processes.

We report the performance of three close-focus microendoscopic distal optical systems. Each system utilized the same aperture stop placed in front of the distal optical element and the same fiber bundle, proximal optical system, and camera. First, a custom-pitch GRIN singlet was designed, modestly decreasing the usual several-millimeter WD to 1.5 mm. Then, to effect very short WDs, two different monolithic 3D-printed glass optical systems, a doublet and triplet, were designed and fabricated.

2 Methods

2.1 *Design Goals*

For best performance in our microendoscopic application, the image must remain in focus for tissue very close to the endoscope (WD less than or equal to 2 mm), the AFOV should be greater than or equal to 40 deg, and DOF should be >1 mm. Saline will be flushed to irrigate the lumen, clear the mucus, and/or displace cilia or plicae ahead of the endoscope, therefore the distal optical system's WD will be in 0.9% saline immersion. The overall system object space resolution requirement is driven by the ability to detect disease. For example, in the fallopian tubes, serous tubal intraepithelial carcinomas (STICs) may be as small as few hundred cells in size.[19] An object space resolution of 20 μm may be sufficient to detect altered optical signatures of STICs and many other diseases. These goals are summarized in Table 1.

2.2 *Distal Optic System Specifications*

The specifications of the three distal optic systems utilized in this study are listed below in Table 2.

Table 1 Design goals for close-focus microendoscopic system.

Optical specification	Goal
WD	<2 mm in 0.9% saline
AFOV	>40 deg
DOF	>1 mm
Resolution	≤ 20 μm

Table 2 Distal optic system designed specifications.

Distal optic system	Diameter (μm)	WD (mm)	Material
Custom GRIN singlet	500	1.5	Nontoxic silver-based glass
3D-printed doublet	500	0.5	Pure silica glass
3D-printed triplet	500	0.4	Pure silica glass

2.3 *Optical Modeling*

The three 0.5-mm distal optic systems were modeled using OpticsStudio (Zemax); custom length GRIN singlet utilizing a glass catalog GRIN lens material (GTAGNEU, GRINTech), and two different custom multielement 3D-printed lenses, a doublet, and triplet. For the GRIN singlet, manufacturer's information about dispersion as a function of wavelength was imported into the material library of OpticStudio and used to model the custom lenses. The GRIN lens rod length (pitch) was allowed to vary, whereas OpticStudio optimized for the smallest spot size with a WD of 1.5 mm. A GRIN rod length of 1.28 mm yielded the best results. For the 3D-printed lens, the LSR was modeled to have a constant index of refraction of 1.44 at 550 nm. The flexibility of the 3D printing process allowed for aspheric surfaces up to the sixth order term. As a result of the optimization process, two potential solutions were devised, a doublet with a nominal WD of 0.5 mm and a triplet with a nominal WD of 0.4 mm. The simpler monolithic doublet contains a stop aperture mount and two biconvex lenses with aspheric surfaces. The more complex monolithic triplet is designed to bring the WD even closer, and push the limits of the 3D printing process, as well as achieve excellent off-axis performance. It contains a stop aperture mount, and three lenses with aspheric surfaces, a biconvex, meniscus, and planoconvex lens. The distal optic system layouts and modulation transfer function (MTF) plots of the three systems are shown in Fig. 1. Our system utilizes a 10,000 element fiber bundle (PN: FIGH-10-350S, Fujikura) with a core-to-core spacing of 3.3 μm, which serves as the limit of the intermediate image space resolution. This fiber bundle's limit is indicated as a vertical line in the MTF plots.

Based on the MTF, the theoretical best on-axis image space resolution of the GRIN singlet, 3D-printed doublet and 3D-printed triplet should be 3.015, 1.485, and 1.656 μm, respectively (with 10% contrast held as the threshold), much better than the fiber bundle's 3.3-μm resolution limit. To increase the DOF of all distal optic systems, the entrance pupil diameter (EPD) was reduced to 250 μm by use of an optical stop at the front of the first surface.

2.4 *3D-Printing Process*

The custom-length GRIN singlet was obtained from GRINTech. The 3D-printed doublet and triplet were manufactured in the precision freeform optics design, fabrication, and testing facility at the University of Arizona via a two-photon polymerization (2PP) technique described previously.[17,20] The technique uses a specially formulated, solvent-free, and photosensitive LSR that has been modified to reduce organic components that cause shrinkage during pyrolysis. Although the described process reduces shrinkage of the printed optic during pyrolysis, multiple trials were still required to determine the prepyrolysis dimensions that achieved the correct post-pyrolysis dimensions. It is critical to complete the pyrolysis process, as this heat treatment

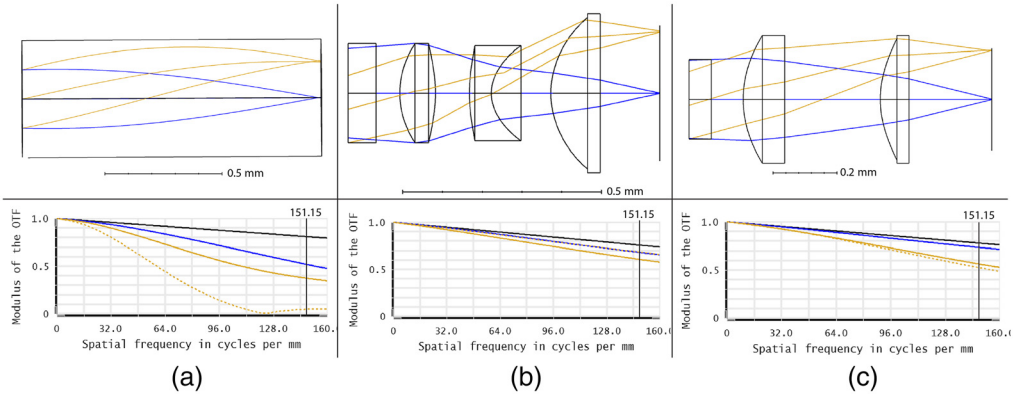

Fig. 1 Distal optic layout and MTFs for (a) GRIN singlet, (b) 3D-printed doublet, and (c) 3D-printed triplet. The blue lines represent the on-axis field, and the golden rays represent the off-axis field (sagittal rays are represented by the dotted lines and tangential rays by the solid lines). The vertical line on the MTF plots signifies the frequency cutoff imposed by the fiber bundle's core-to-core spacing (3.3 μm) converted to lps per mm (151.2 lp/mm).

vaporizes the organic molecules that absorb shorter wavelengths, which cause a yellowish cast in the images. Figure 2 displays the transmittance of the prepyrolysized and postpyrolysized material in the visible spectrum.

The LSR was polymerized by the 2PP system consisting of a 0.6 NA objective, 780-nm fs laser, 1.4 nJ pulse energy, and 75 mm/s scanning speed. The 2PP setup is shown in Fig. 3. The doublet and triplet systems were manufactured in 1.5 and 3 hrs, respectively, and the latter has greater structural complexity and number of elements. Figure 4 shows photographs of the two 3D-printed distal optic systems mounted on the fiber bundle, as well as electron micrographs of the systems before experimentation.

2.5 *Experimental Setup*

To create the EPD of 250 μm, the system stop, a blackened, stainless steel microwasher (Gateway Laser) with outer diameter 500 μm and inner diameter 250 μm was glued to the front face of each lens using UV-curing glue (PN: NOA68, Norland). The test bench setup consisted of resting the distal optic system in a stainless-steel V-groove holder and abutting the 10,000 element fiber bundle (PN: FIGH-10-350S, Fujikura) against the lens in the V-groove. The

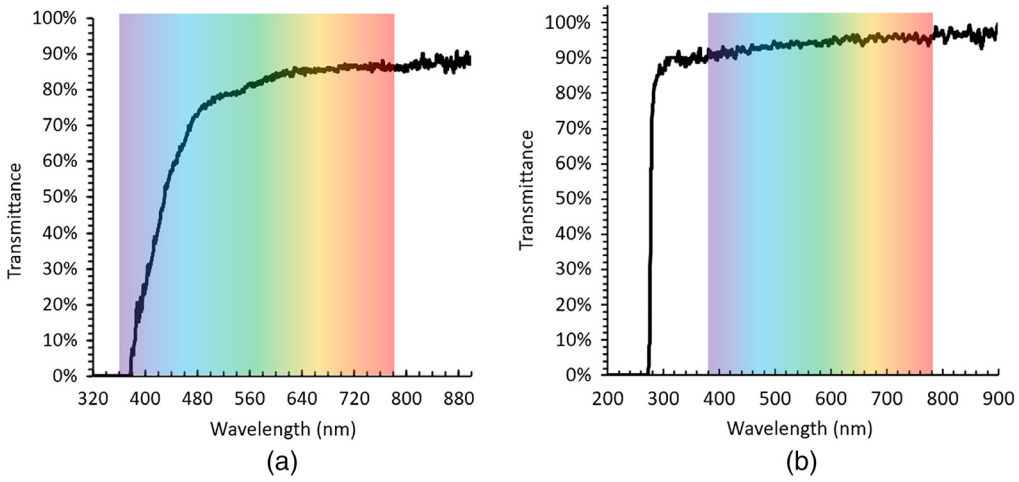

Fig. 2 Transmittance of (a) the prepyrolysis LSR and (b) postpyrolysis LSR in the visible spectrum.

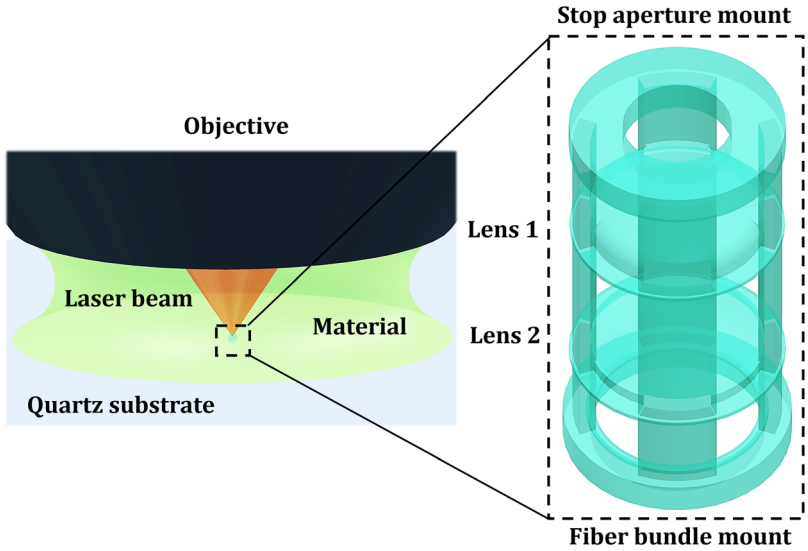

Fig. 3 Schematic of the 2PP-enabled 3D-printing setup and printing process.

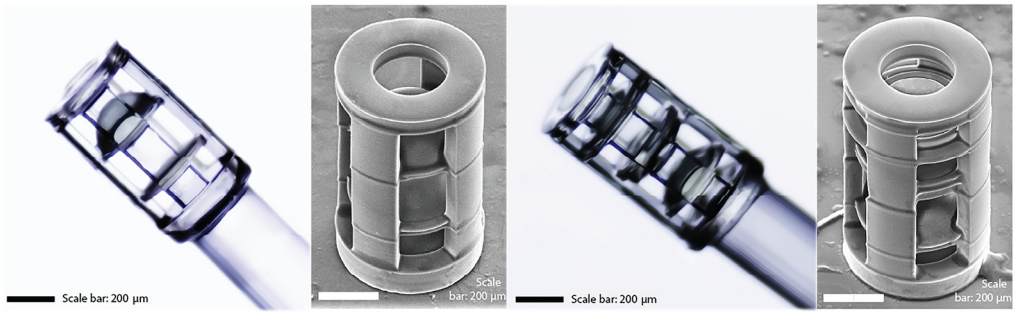

Fig. 4 (a) and (b) Photographs and electron micrographs of 3D-printed doublet and (c) and (d) triplet. Scale bar is 200 μm.

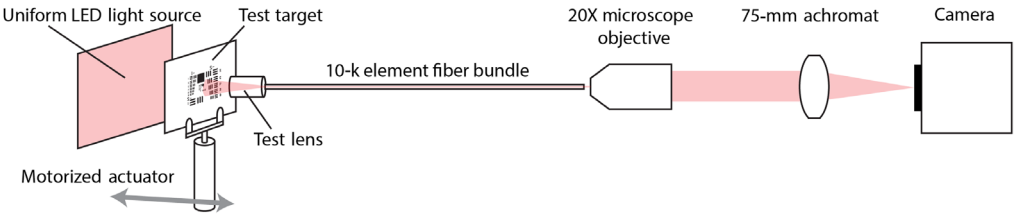

Fig. 5 Diagram of test setup.

opposite end of the fiber bundle was positioned at the WD of a 20× microscope objective (PN: UAPON20XW340, Olympus), whose image was then magnified by a 75-mm focal length achromat lens (PN: AC254-075-A, Thorlabs) onto a CMOS detector (PN: ON Semi PYTHON 1300BFS-U3-13Y3C-C, Teledyne FLIR) with auto-exposure activated. SpinView software (Spinnaker SDK, Teledyne FLIR) was used to display and save the images. For testing, a 3″ × 3″ positive variable line grating (R1L3S6P, Thorlabs), a 3″ × 3″ 1951 United States Air Force (USAF) Resolution Test Target (DA004, MaxLevy/II-VI), or a 100-μm grid target (R1L3S3P, Thorlabs) was positioned at the WD of the distal optic system and translated by motorized linear actuator (T-NA08A25, Zaber). The test target was back-illuminated by a large uniform light emitting diode (LED) source (CX Series, Advanced Illumination). Images were taken of different lp/mm resolution patterns at each object distance. These images were used to obtain the as-built WD, AFOV, DOF, distortion, and object space resolution of each test lens. Figure 5 illustrates the testing setup.

To obtain the as-built WD, the test target was moved to the position of highest contrast. To obtain the object size or field of view (FOV), images of the 26 lp/mm resolution pattern were collected at the WD. The number of line pairs (lps) visible in each image was counted and divided by 26 to obtain the FOV in mm. With the knowledge of the as-built WD, the FOV was also translated into AFOV via geometric calculations.

To obtain DOF and object space resolution, the images were analyzed in ImageJ (National Institutes of Health, United States). The DOF was determined as the range of object distances over which the object, in this case the 26 lp/mm grating, remained resolvable to ∼10% contrast. To calculate contrast, the average grayscale intensity of a sample of pixels in 3 to 4 fiber bundle cores imaging "white" (transparent) sections of the line grating was measured. Similarly, the average grayscale intensity of cores imaging "black" (opaque) locations was measured. These values were then used in the following contrast equation:

$$C = \frac{(I_{\max} - I_{\min})}{(I_{\max} + I_{\min})}.$$

To determine the resolution of the distal optic system, the line grating was swapped out for the 1951 USAF Target. For this study, resolution was defined as the smallest group and element of the USAF Target that could be resolved with ∼10% contrast, at the lens WD. According to MTF

plots (a), (b), and (c) in Fig. 1, the 10,000-element fiber bundle, rather than the distal optic system, is the limiting factor on overall system resolution, where each fiber core-to-core spacing in the bundle serves as the intermediate blur diameter criterion for the overall system. Therefore, the as-built theoretical best resolution due to the distinct cores of the fiber bundle was calculated by dividing the FOV (mm) by the number of cores across the diameter of the fiber bundle. This value describes the object size that corresponds to 1 fiber core. Any object below the as-built theoretical limit will not be distinguishable through the fiber bundle system. Note that each "fiber pixel" at the proximal end of the fiber bundle was imaged on to the camera with sufficient camera pixels to ensure that detector resolution is not a limiting factor.

3 Results

The WD, FOV, AFOV, DOF, and resolution observed for each lens is collated in Table 3 below. The theoretical resolution limit due to the fiber bundle is also provided. Barrel distortion is evident in the images, of ~8.3%, 5.0%, and 3.5% at the edge of the field of view for the GRIN, 3D-printed doublet, and 3D-printed triplet, respectively.

3.1 *Working Distance and Full Field of View*

The as-built WDs of the GRIN singlet, 3D-printed doublet, and 3D-printed triplet were 1.30, 0.81, and 0.55 mm, respectively. The FOV and AFOV of each distal optic system was 1.19, 1.00, and 0.731 mm, or 49.3 deg, 63.4 deg, and 67.2 deg, respectively. Figure 6 shows images taken with each system of the 26 lp/mm test pattern at the WD to qualitatively illustrate the differences in FOV at WD, color rendition, and image contrast.

The FOV (mm) of the GRIN singlet is greater than the 3D-printed doublet or triplet systems, even though it has a smaller AFOV. This is unsurprising, as the object was held at the WD of

Table 3 As-built result comparison.

Distal optic system	WD (mm)	FOV (mm)	AFOV (deg)	DOF (mm)	Measured resolution (μm)	Theoretical resolution limit (μm)
Goal	≤ 2		>40	>1.0	<20	
Custom GRIN singlet	1.30	1.19	49.3	0.70	9.84	12.11
3D-printed doublet	0.81	1.00	63.4	0.71	8.77	10.15
3D-printed triplet	0.55	0.731	67.2	0.55	17.54	7.42

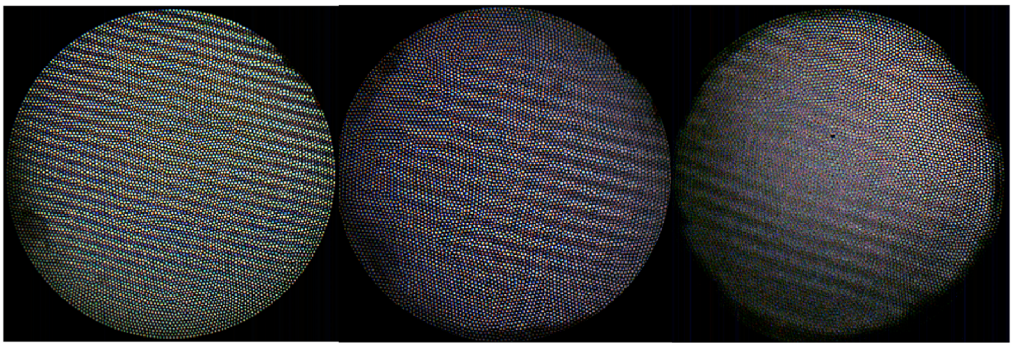

(a) (b) (c)

Fig. 6 Images of the 26 lp/mm resolution pattern taken at the lens-specific WD for the (a) GRIN singlet, (b) 3D doublet, and (c) 3D triplet.

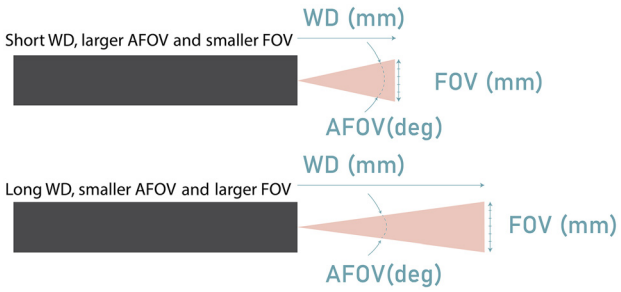

Fig. 7 Diagram depicting how a lens with a smaller AFOV but larger WD can result in a larger FOV than a lens with a larger AFOV and shorter WD.

each lens, of which the GRIN singlet has the largest. Figure 7 illustrates how a lens with a smaller AFOV but larger WD can have a larger FOV than a lens with a larger AFOV. It is instructive to compare the object AFOV in degrees, as it is the more analogous measurement. The 3D doublet and triplet have similar AFOV (63.4 deg and 67.2 deg, respectively) with the GRIN singlet having the smallest AFOV at 49.3 deg.

3.2 *Depth of Field*

The GRIN singlet and 3D-printed doublet featured almost identical DOFs of 0.7 and 0.71 mm, respectively with respective object distance ranges of 0.9 to 1.6 mm and 0.5 to 1.21 mm. The 3D-printed triplet had a DOF of 0.55 mm from 0.30 to 0.85 mm.

3.3 *Resolution*

At the distal optic system's WD, it was possible to visualize, with 10% contrast or greater, group 5 element 5, group 5 element 6, and group 4 element 6, for the GRIN, 3D-printed doublet, and 3D-printed triplet lens, respectively. This corresponds to a spatial resolution of 9.84, 8.77, and 17.54 μm, respectively (Fig. 8).

3.4 *Performance in a Microscope System*

To qualitatively assess the performance of the distal optic systems without the resolution limitations of the fiber bundle, a 10×, 0.25 NA microscope was used to observe the intermediate image formed by the GRIN singlet and 3D-printed doublet and triplet. The collected images of a histology section of fallopian tube (formalin fixed, paraffin embedded, 6-μm-thick section,

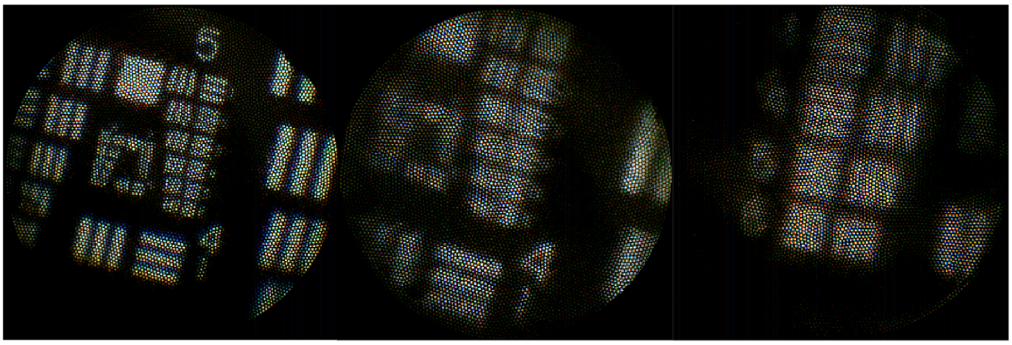

Fig. 8 Images of the USAF target taken at the corresponding WDs for the (a) GRIN singlet showing group 5, (b) 3D-printed doublet showing group 5, and (c) 3D-printed triplet showing group 4 elements 4, 5, and 6.

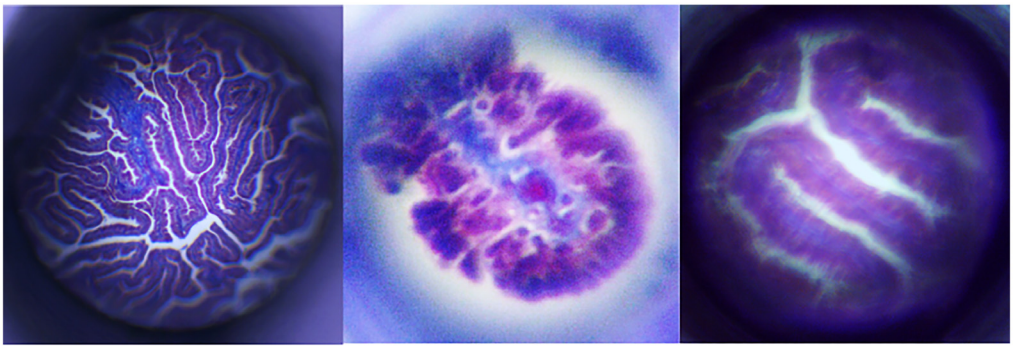

Fig. 9 Images of a histological slide of human fallopian tissue taken in a microscope setup with the (a) GRIN singlet, (b) 3D-printed doublet, and (c) 3D-printed triplet.

stained with hematoxylin and eosin) are shown in Fig. 9. The large differences in FOV are evident, although visualization of plicae is possible with all.

4 Discussion

This study characterized the properties of three 0.50-mm-diameter distal optic systems for close-focus microendoscopic use. Table 3 compares the performance of the three distal optic systems against the goals set. All distal optic systems exceeded WD and AFOV expectations. However, none of the distal optic systems were able to achieve a DOF >1 mm. It is promising that the 3D-printed doublet's DOF (0.71 mm) was almost identical to the DOF performance of the GRIN singlet (0.7 mm). Typically, the extremely close focus (0.81 and 0.55 mm) of the two 3D-printed systems compared to the GRIN singlet (1.30 mm) would cause a greater tradeoff in DOF, as seen in the 3D-printed triplet. This would be expected, since the EPD of all lenses was the same (0.250 mm), the object space numerical aperture is much higher for the 3D-printed lenses, typically leading to a concurrent decrease in DOF. All lenses had a measured resolution poorer than the highest predicted by the MTF at 10% contrast. However, the GRIN singlet and 3D doublet had resolved test patterns close to that predicted based on the limit imposed by the fiber bundle. The slightly better measured, compared to as-built theoretical, resolution of the GRIN singlet and 3D-printed doublet may be due to small measurement error or a fiber bundle with core-core spacing smaller than that specified by the manufacturer. The 3D-printed triplet had poorer than expected resolution performance. It is possible that this very complex lens suffered from a final manufactured shape that deviated from design. Some core-to-core color variations are seen in all images. If desired, the transmission intensity and color variations between fiber cores could be corrected by calibration using an image of a uniformly bright white target (a "flat" image).[21]

CMOS detectors are now available with submicron size pixels. As overall sensor sizes shrink and number of pixels increases, miniature sensors should become more prevalent in microendoscopes. The resolution of these future optical systems may no longer be limited by a fiber element or pixel size; the limiting element will be the distal optic system. The wide availability and simplicity of the GRIN singlets makes it a current favorite for microendoscopic use.[22,23] However, GRIN singlets lack the versatility of 3D-printed monolithic optical systems, which can be designed for extremely short WDs and to mitigate aberrations. 3D-printed optical systems also have greater potential for multimodality use, with, e.g., multifocal capability.[15] The ability to integrate mounting surfaces in a monolithic design, including fiber bundle and aperture stop mounts, is a unique capability that can greatly ease assembly. Ongoing research in glass printing techniques is leading to more accurate/predictable shapes after processing. As a result, sub-millimeter endoscopes with a close focus will become feasible for imaging small and collapsed lumens such as the Eustachian tube, pancreatic ducts, or tear ducts. Overall, this study provides further evidence that 3D-printed lenses are a promising option for extending the capabilities of microendoscopes.

Acknowledgments

The research reported in this publication was supported by the National Cancer Institutes of Health (Grant Nos. R01CA260399, 1R21CA229707, and 5U01CA200469). The authors declare that there are no conflicts of interest related to this article.

References

1. C. Kahi et al., "Colonoscopy and colorectal cancer mortality in the veterans affairs health care system: a case-control study," *Ann. Intern. Med.* **168**(7), 481–488 (2018).
2. A. Kano et al., "Microendoscopes for imaging of the pancreas," *Proc. SPIE* **5318**, 50–58 (2004).
3. J. Kerin et al., "Falloposcopy: a microendoscopic technique for visual exploration of the human fallopian tube from the uterotubal ostium to the fimbria using a transvaginal approach," *Fertil. Steril.* **54**(3), 390–400 (1990).
4. L. Thiberville et al., "In vivo imaging of the bronchial wall microstructure using fibered confocal fluorescence microscopy," *Am. J. Respir. Crit. Care Med.* **175**(1), 22–31 (2007).
5. G. Hohert et al., "Feasibility of combined optical coherence tomography and autofluorescence imaging for visualization of needle biopsy placement," *J. Biomed. Opt.* **25**(10), 106003 (2020).
6. W. Göbel et al., "Optical needle endoscope for safe and precise stereotactically guided biopsy sampling in neurosurgery," *Opt. Express*, **20**(24), 26117–26126 (2012).
7. T. H. Tate et al., "Ultraminiature optical design for multispectral fluorescence imaging endoscopes," *J. Biomed. Opt.* **22**(3), 036013 (2017).
8. Y. Yang et al., "A two-step grin lens coating for in vivo brain imaging," *Neurosci. Bull.* **35**(3), 419–424 (2019).
9. M. Keenan et al., "Design and characterization of a combined oct and wide field imaging falloposcope for ovarian cancer detection," *Biomed. Opt. Express* **8**(1), 124–136 (2016).
10. K. C. Kiekens et al., "Reengineering a falloposcope imaging system for clinical use," *Transl. Biophotonics* **2**, e202000011 (2020).
11. M. W. Lee et al., "Astigmatism-corrected endoscopic imaging probe for optical coherence tomography using soft lithography," *Opt. Lett.* **45**, 4867–4870 (2020).
12. A. Antonini et al., "Extended field-of-view ultrathin microendoscopes for high-resolution two-photon imaging with minimal invasiveness," *elife* **9**, e58882 (2020).
13. H. Pahlevaninezhad et al., "Nano-optic endoscope for high-resolution optical coherence tomography in vivo," *Nat. Photonics* **12**(9), 540–547 (2018).
14. J. Li et al., "Ultrathin monolithic 3D printed optical coherence tomography endoscopy for preclinical and clinical use," *Light: Sci. Appl.* **9**, 124 (2020).
15. J. Li et al., "3D-printed micro lens-in-lens for in vivo multimodal microendoscopy," *Small* **18**(17), 2107032 (2022).
16. K. C. Kiekens and J. K. Barton, "3D printed lens for depth of field imaging," *OSA Contin.* **2**(11), 3019–3025 (2019).
17. Z. Hong et al., "Three-dimensional printing of glass micro-optics," *Optica* **8**(6), 904–910 (2021).
18. Z. Hong et al., "High-precision printing of complex glass imaging optics with precondensed liquid silica resin," *Adv. Sci.* **9**, 2105595 (2022).
19. J. D. Seidman, "Serous tubal intraepithelial carcinoma localizes to the tubal-peritoneal junction: a pivotal clue to the site of origin of extrauterine high-grade serous carcinoma (ovarian cancer)," *Int. J. Gynecol. Pathol.* **34**(2), 112–120 (2015).
20. W. Kang, Z. Hong, and R. Liang, "3D printing optics with hybrid material," *Appl. Opt.* **60**(7), 1809–1813 (2021).
21. S. J. Olivas et al. "Fiber bundle image relay for monocentric lenses," in *Classical Opt.*, p. CTh1C.5 (2014).
22. W. M. Lee and S. H. Yun, "Adaptive aberration correction of GRIN lenses for confocal endomicroscopy," *Opt. Lett.* **36**, 4608–4610 (2011).

23. R. P. Barretto et al., "Time-lapse imaging of disease progression in deep brain areas using fluorescence microendoscopy," *Nat. Med.* **17**(2), 223–228 (2011).

Dominique Galvez received her BS degree in optical sciences and engineering from the University of Arizona. She is pursuing a PhD in optical sciences at the University of Arizona researching microendoscopes, 3D-printed optics, endoscopic OCT, multimodal imaging, and endoscopic cell collection.

Jennifer K. Barton, PhD, is working as a Thomas R. Brown distinguished chair in engineering, professor of biomedical engineering, and director of the BIO5 Institute at the University of Arizona. Her research interests include development of miniature multimodality optical endoscopes and light-tissue interaction. She is a fellow and 2023 president-elect of SPIE.

Biographies of the other authors are not available.